Available online at www.sciencedirect.com
ScienceDirect
Journal of Catalysis 247 (2007) 34–42
JOURNAL OF CATALYSIS
www.elsevier.com/locate/jcat

Evidence for Rh electron-deficient atoms ($Rh^{\delta+}$) as the catalytic species for CO oxidation when supported on $Ce_{0.68}Zr_{0.32}O_2$: A combined N_2-FTIR, benzene hydrogenation, and kinetic study

Céline Fontaine-Gautrelet [1], Jean-Marc Krafft, Gérald Djéga-Mariadassou, Cyril Thomas *

Laboratoire de Réactivité de Surface, UMR CNRS 7609, Université Pierre et Marie Curie – Paris 6, 4 Place Jussieu, Case 178, 75252 Paris cedex 05, France

Received 20 November 2006; revised 10 January 2007; accepted 10 January 2007

Available online 12 February 2007

Abstract

The characterization of two low-loaded Rh(wt%)/$Ce_{0.68}Zr_{0.32}O_2$ samples (Rh(0.29)/CZ and Rh(0.32)/CZ) was performed via N_2-FTIR and benzene hydrogenation before being investigated for CO oxidation activity and kinetics. N_2-FTIR allows characterization of both $Rh^{\delta+}$ ($\nu_{N_2} = 2295\ cm^{-1}$) and Rh^0 ($\nu_{N_2} = 2192\ cm^{-1}$) centers and revealed that the concentration of $Rh^{\delta+}$ does not vary to a significant extent on both samples, whereas the concentration of Rh^0 sites increases dramatically on Rh(0.32)/CZ, as also supported by benzene hydrogenation activities. In contrast, CO oxidation activity and kinetics are nearly identical on both catalysts. This clearly indicates that CO oxidation is catalyzed not by the Rh^0 centers, but more likely by the $Rh^{\delta+}$ centers. Such a conclusion is supported by the estimated reaction orders with respect to CO and O_2, which are obviously different from those expected for Rh^0 catalytic sites. The dramatic increase in the concentration of the Rh^0 centers on Rh(0.32)/CZ suggests the presence of electron-enriched Rh clusters on Rh(0.29)/CZ, owing to the basicity of CZ. These electron-enriched Rh clusters, which neither catalyze benzene hydrogenation nor chemisorb N_2, do not catalyze CO oxidation either.

Keywords: Benzene hydrogenation; N_2-FTIR; O_2 pulse; Rh catalysts; Ceria–zirconia; CO oxidation; Basicity

1. Introduction

Three-way catalysts (TWC) would not have been the well-known success story in the purification of gasoline engine exhausts if CeO_2, and later $Ce_xZr_{1-x}O_2$ mixed oxides, had not been added to the TWC formulations [1]. These CeO_2-based oxides, which exhibit unique oxygen storage–release properties [2] depending mainly on the gaseous atmosphere with which they are in contact [1], are key components of the TWC. Under TWC lean-rich oscillating operating conditions, these oxides help maintain elevated CO and unburnt HC oxidation efficiencies, even in the rich incursions required to achieve improved NO_x conversion, by providing extra oxygen stored under the lean periods [1].

The constant improvement of TWC formulations also revealed the need for intimate contact between the CeO_2-based oxides and the platinum group metals (PGMs: Rh, Pt, and Pd) to ensure enhanced pollutant removal [1]. It is noteworthy that such intimate contact may alter the oxidation state of the deposited PGMs [3,4].

For the CO oxidation reaction, it has been widely reported that this catalytic reaction is greatly promoted by the incorporation of CeO_2-based oxides [5–17]. Although Yu Yao concluded, more than 20 years ago [6], that two types of surface sites (zero-valent and oxidized) may be considered to explain the striking differences observed in CO–O_2 kinetics on CeO_2-promoted PGMs samples compared with nonpromoted ones, few authors attributed the enhanced catalytic activity of the CeO_2-promoted PGMs catalysts to the presence of oxidized

* Corresponding author. Fax: +33 1 44 27 60 33.
E-mail address: cthomas@ccr.jussieu.fr (C. Thomas).
[1] Present address: CenTACat, Queen's University Belfast, Belfast BT9 5AG, N. Ireland, UK.

0021-9517/$ – see front matter
doi:10.1016/j.jcat.2007.01.005

PGM species [14–19]. This peculiarity may arise from the fact that in most studies [6–13], both zero-valent and oxidized surface species coexist on the studied catalysts and that the available characterization methods usually focus on the titration of the zero-valent species only, so that the presence of the oxidized species is most often ignored.

In previous studies [15,17], we inferred the differences in CO–O_2 kinetics observed between a Rh(0.29)/$Ce_{0.68}Zr_{0.32}O_2$ (Rh(0.29)/CZ) catalyst and a Rh/SiO_2 reference catalyst to the reactivity of Rh oxidized species, as the model benzene hydrogenation reaction, which titrates only Rh^0 sites [20–22], proceeded to a very limited extent on Rh(0.29)/CZ. Very recently, characterization of Rh(0.29)/CZ through the adsorption of CO and N_2 molecular probes followed by FTIR confirmed the presence of oxidized Rh species even after reduction under H_2 at 500 °C [23]. In this work, it was concluded that Rh was stabilized mainly as electron-deficient clusters ($Rh_n^{\delta+}$) on Rh(0.29)/CZ. The existence of these species may be caused by either electron perturbation induced on the metal by the reduced support [24] or, more likely, electron withdrawal from the metal clusters by an inductive effect of the neighboring Cl anions [25–28]. In the presence of CO, however, evidence of $Rh^I(CO)_2$ species was also provided, the formation of which results from the well-known oxidative disruption of the Rh^0 clusters assisted by the neighboring OH groups [29–35]. Nevertheless, the catalytic reactivity of $Rh^I(CO)_2$ species for CO oxidation is fairly low [36–39], leading us to conclude that the activity of the Rh(0.29)/CZ catalyst [17] is presumably due to the $Rh^{\delta+}$ sites [39].

This work aims at providing additional evidence for the fact that $Rh^{\delta+}$ sites supported on $Ce_{0.68}Zr_{0.32}O_2$ are the catalytic sites responsible for the enhanced CO oxidation activity of $Ce_{0.68}Zr_{0.32}O_2$-supported Rh catalysts. For this purpose, a Rh/CZ catalyst with a nominal content of Rh close to that of the material studied previously [17] was synthesized. The synthesis of this catalyst was realized on a precalcined CZ support, however, to significantly increase the fraction of Rh^0 sites. Both of these catalysts were characterized through the benzene hydrogenation model reaction and adsorption of N_2 followed by FTIR (N_2-FTIR). These techniques allowed characterization of the Rh^0 sites, whereas N_2-FTIR also revealed the presence of $Rh^{\delta+}$ species. Finally, CO–O_2 transient experiments and steady-state kinetics were performed on the newly synthesized catalyst and compared with those obtained previously on Rh(0.29)/CZ [17].

2. Experimental

2.1. Catalyst preparation

The two low-loaded Rh/CZ catalysts (0.29 [17] or 0.32 wt% Rh) were prepared by anionic exchange from an acidic solution of $RhCl_3{\cdot}3H_2O$ (Johnson Matthey) with the ceria–zirconia ($Ce_{0.68}Zr_{0.32}O_2$: CZ, ∼200 $m^2\,g^{-1}$) support [18]. The acidic solution of $RhCl_3{\cdot}3H_2O$ (7.8×10^{-3} mol L^{-1}) was added to 80 cm^3 of an aqueous suspension of 2.5 g of CZ previously set to pH 1.9 by the addition of HCl. After undergoing exchange for 15 min under vigorous stirring, the Rh/CZ catalyst was filtered and washed with distilled water before drying in air at room temperature for 12 h and then at 120 °C for 3 h. It is noteworthy that Rh(0.29)/CZ was synthesized from the uncalcined CZ support, whereas the CZ support was calcined under air at 500 °C for 2 h before synthesis of Rh(0.32)/CZ.

For comparison, two additional catalysts were prepared. A chlorided-CZ material was synthesized by submitting the uncalcined CZ support to an identical acidic treatment as that of the above-mentioned low-loaded Rh/CZ catalysts. The chlorided-CZ material was then filtered and washed with distilled water before drying in air at room temperature for 12 h and at 120 °C for 3 h. A Rh/CZ catalyst with a greater Rh loading (1.45 wt%) was prepared by incipient wetness impregnation of the chlorided-CZ material by an aqueous solution of $RhCl_3{\cdot}3H_2O$ (0.31 mol L^{-1}) and subsequently dried in air at room temperature for 12 h and at 120 °C for 3 h.

Rh and Cl contents were determined, after reduction under H_2 at 500 °C for 2 h, by chemical analyses (CNRS, Vernaison, France). The results of the chemical elemental analyses, given in Table 1, show that the Cl contents of CZ, Rh(0.29)/CZ, and Rh(0.32)/CZ are close to 1 wt%, whereas that of Rh(1.45)/CZ is about 2 wt%. The greater Cl content of Rh(1.45)/CZ agrees well with the fact that this material was not washed with distilled water after impregnation.

The specific surface areas were determined by physisorption of N_2 at −196 °C using a Quantasorb Jr. dynamic system equipped with a thermal conductivity detector (TCD). The specific surface areas were calculated using the BET method. Table 1 shows that the specific surface areas of CZ, Rh(0.29)/CZ, and Rh(1.45)/CZ are scarcely affected (<10% of the initial surface) by the Cl and Rh deposition processes, whereas thermal treatments in flowing air or H_2 at 500 °C for 2 h lead to a substantial decrease (about 35%) in specific surface area. For

Table 1
Chemical elemental analyses, specific surface areas and benzene hydrogenation activities of the studied $Ce_{0.68}Zr_{0.32}O_2$-based catalysts reduced under flowing H_2 at 500 °C for 2 h

Catalysts	Rh (wt%)	Cl (wt%)	Specific surface area ($m^2\,g^{-1}$)		Benzene hydrogenation activity	
			Post-synthesis	Reduced at 500 °C	10^{-6} mol s^{-1} g_{cat}^{-1}	10^{-6} mol s^{-1} g_{Rh}^{-1}
CZ[a]	0.00	1.06	191	135	0	0
Rh/CZ[a]	0.29	0.95	185	130	0.18	65
Rh/CZ[b]	0.32	1.11	129	122	1.99	622
Rh/CZ[a]	1.45	1.65	186	143	5.45	375

[a] Synthesized from uncalcined $Ce_{0.68}Zr_{0.32}O_2$.
[b] Synthesized from $Ce_{0.68}Zr_{0.32}O_2$ calcined at 500 °C for 2 h.

Rh(0.32)/CZ, the subsequent reduction step does not produce a further significant decrease in the specific surface area of the precalcined support.

2.2. Benzene hydrogenation

Because of the well-known reducibility of the CZ support [40], which makes the use of the common chemisorption techniques difficult, the presence of exposed zero-valent Rh atoms (Rh^0) was revealed by means of the benzene hydrogenation reaction [21,22]. Before benzene hydrogenation, the catalyst sample (0.050 g deposited on a plug of quartz wool inserted inside a Pyrex reactor) was heated in flowing H_2 (100 $cm^3_{NTP}\,min^{-1}$) at atmospheric pressure with a heating rate of 3 °C min^{-1} up to 500 °C and held at this temperature for 2 h. After cooling to 50 °C under H_2, the reaction was started. The partial pressure of benzene was 51.8 Torr (1 Torr = 133 Pa), and the total flow rate was 107 $cm^3_{NTP}\,min^{-1}$ with H_2 as balance.

The composition of the effluent was analyzed using an online gas chromatograph (Hewlett Packard 5890, FID) equipped with a PONA (paraffins–olefins–naphthenes–aromatics; HP, 50 m long, 0.20 mm i.d., 0.5 μm film thickness) capillary column. Cyclohexane was the only product detected.

2.3. Low-temperature N_2 adsorption followed by FTIR

Fourier transform infrared (FTIR) spectra of adsorbed N_2 on the CZ-based samples were collected on a Bruker Vector 22 FTIR spectrometer equipped with a liquid N_2-cooled MCT detector and a data acquisition station. A total of 256 scans were averaged with a spectral resolution of 2 cm^{-1}.

The samples were pressed into self-supporting wafers of 8–14 mg cm^{-2}. The wafers were loaded in a moveable glass sample holder, equipped on top with an iron magnet, and inserted in a conventional Pyrex-glass cell (CaF_2 windows) connected to a vacuum system. The iron magnet allowed for the transfer of the catalyst sample from the oven-heated region to the infrared light beam. The glass cell was placed in a polystyrene container that allowed the sample to be cooled to a temperature of about −173 °C with liquid N_2.

Before N_2 adsorption, the catalysts were submitted to a dynamic (50 $cm^3\,min^{-1}$) reducing pretreatment (5% H_2 in Ar, Air Liquide, 99.999%) at 500 °C for 2 h at atmospheric pressure. The samples were then evacuated (7.5×10^{-7} Torr) at 500 °C for 60 min. Finally, the temperature was decreased to −173 °C under dynamic vacuum. To ensure adequate cooling of the sample, a pulse of 0.1 μmol of He (Air Liquide, 99.999%) was introduced. The samples were contacted to N_2 (Air Liquide, 99.999%) under a pressure of about 16 Torr and pulses of O_2 (Air Liquide, 99.999%) were then introduced on the N_2-preadsorbed samples as described previously [41].

Unless specified otherwise, the spectrum at −173 °C of the pretreated sample was used as a reference and subtracted from the spectra of the sample exposed to the different probe molecules. For all spectra, absorbances have been normalized with respect to the sample weight.

2.4. CO oxidation experiments

Before runs, the catalyst samples (0.200 g, 125–200 μm) were submitted to a temperature-programmed reduction from room temperature to 500 °C (3 °C min^{-1}) under H_2 (Air Liquide, 100 $cm^3_{NTP}\,min^{-1}$) and held at this temperature for 2 h. After pretreatment, the catalysts were flushed at 500 °C for 15 min under helium (230 $cm^3_{NTP}\,min^{-1}$), and the catalyst temperature was decreased to room temperature. Before kinetic measurements, two subsequent and reproducible CO–O_2 (0.4–0.2% in He, 230 $cm^3_{NTP}\,min^{-1}$ total flow rate) temperature-programmed reactions were carried out from room temperature to 500 °C at a heating rate of 3 °C min^{-1} to ensure the reliability of the activation procedure.

The kinetic study was conducted in a U-type quartz dynamic differential microreactor (20 mm i.d.). The synthetic gas mixture was fed from independent mass flow controllers (Brooks 5850). The reactor outflow was analyzed using an infrared detector (Maihak 710), allowing for the simultaneous recording of CO and CO_2. CO conversions ($X_{CO} = [CO_2]_T/[CO]_i$, where $[CO_2]_T$ and $[CO]_i$ are the concentration of CO_2 measured at temperature T and the initial concentration of CO, respectively) were calculated.

Because CO oxidation is strongly exothermic, external and internal diffusion limitations were verified under transient experimental conditions [17]. These experiments showed that both internal and external limitations occurred only at CO conversions >60%.

The kinetic parameters reported in the present work were obtained at steady state, while the reactor was operated isothermally and as close to a differential reactor as possible by limiting the conversion to <10%. The CO reaction order was determined at 115 °C under reducing or oxidizing reactive gas mixtures by maintaining the O_2 concentration at 0.20% and varying the CO concentration from 0.44 to 0.40% or from 0.33 to 0.40%, respectively. The O_2 reaction order was determined at 115 °C under reducing or oxidizing reactive gas mixtures by maintaining the CO concentration at 0.40% and varying the O_2 concentration from 0.16 to 0.20% or from 0.33 to 0.20%, respectively. The apparent activation energy was determined with an accuracy of ±10 kJ mol^{-1} under stoichiometric conditions (0.40% CO and 0.20% O_2 in He) at reaction temperatures of 110–125 °C.

3. Results

3.1. Benzene hydrogenation

Table 1 gives the benzene hydrogenation activity of the various samples obtained after reduction in H_2 at 500 °C for 2 h. Among the supported Rh catalysts, this table shows that the benzene hydrogenation rate is the lowest for Rh(0.29)/CZ. It also shows that the calcination of CZ before deposition of Rh has a dramatic influence on the benzene hydrogenation rate, as that estimated on Rh(0.32)/CZ is one order of magnitude greater than that determined on Rh(0.29)/CZ. Finally, the benzene hydrogenation activity of Rh(1.45)/CZ, calculated per

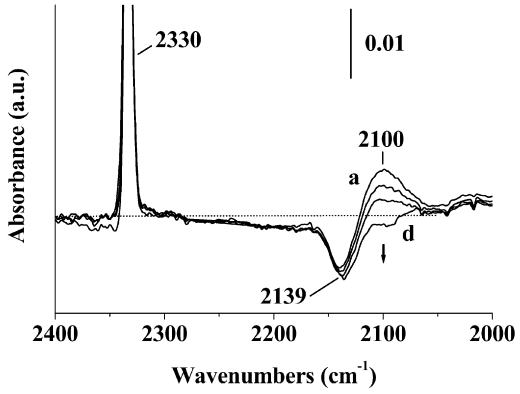

Fig. 1. Low temperature (−173 °C) infrared spectra of the CZ catalyst after adsorption of: (a) N_2 at a pressure of 18.2 Torr and (b–d) subsequent pulses of 0.54, 0.76, and 1.51 μmol of O_2, respectively.

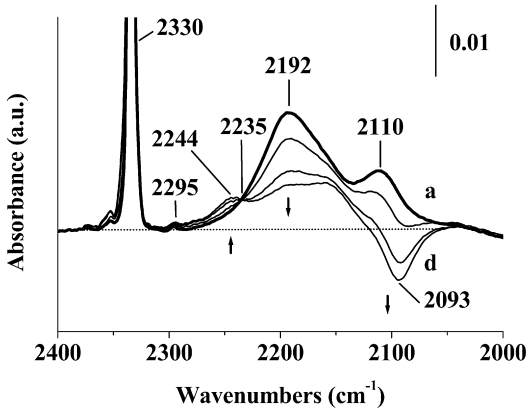

Fig. 2. Low temperature (−173 °C) infrared spectra of the Rh(1.45)/CZ catalyst after adsorption of: (a) N_2 at a pressure of 16.2 Torr and (b–d) subsequent pulses of 1.91, 1.52, and 0.76 μmol of O_2, respectively.

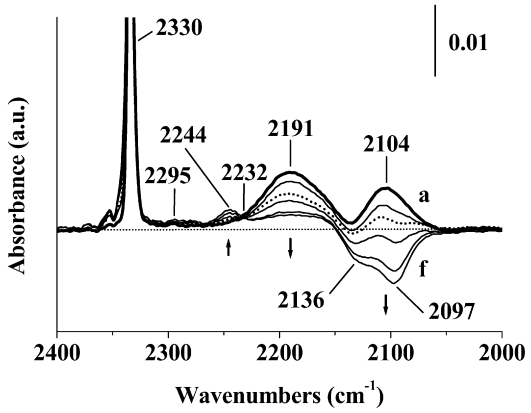

Fig. 3. Low temperature (−173 °C) infrared spectra of the Rh(0.32)/CZ catalyst after adsorption of: (a) N_2 at a pressure of 16.0 Torr and (b, d–f) subsequent pulses of 1.92, 1.42, 2.12, and 0.71 μmol of O_2, respectively. Spectrum c (- - -) was recorded 40 min after measurement of spectrum b without introduction of a new pulse of O_2.

gram of Rh, is about half that of Rh(0.32)/CZ. This result may be reasonably attributed to an increase in Rh particle size and thus to a decrease in the percentage of exposed Rh^0 surface sites compared with Rh(0.32)/CZ.

3.2. Adsorption of N_2 at −173 °C followed by FTIR

As CO may alter the catalytic sites onto which the adsorption occurs [42], characterization of the Rh catalysts by FTIR was done using N_2 as a molecular probe. Studies aimed at characterizing Rh catalysts by means of N_2-FTIR [23,41,43–47] are much less numerous than those performed with CO-FTIR [42], due to the fact that N_2 interacts very weakly with transition metals and the extinction coefficient of adsorbed N_2 is much lower than that of adsorbed CO [45].

3.2.1. CZ

The FTIR spectrum of CZ contacted under 18.2 Torr of N_2 is presented in Fig. 1 (spectrum a). This spectrum shows a narrow, intense absorption band at 2330 cm^{-1}, which can be attributed to N_2 physisorbed on the OH groups of the support [45–47]. Along with this band, negative and positive contributions are also seen at 2139 and 2100 cm^{-1}, respectively.

When O_2 is pulsed on the CZ sample maintained under N_2, the intensities of the absorption band at 2330 cm^{-1} (not shown) and the negative contribution at 2139 cm^{-1} (Fig. 1, spectra b–d) are hardly affected. In contrast, that of the positive contribution at 2100 cm^{-1} clearly decreases after the introduction of small quantities of O_2.

3.2.2. Rh(1.45)/CZ

The FTIR spectrum obtained on Rh(1.45)/CZ after adsorption of N_2 at −173 °C is shown in Fig. 2 (spectrum a). As is the case for CZ, an absorption band is observed at 2330 cm^{-1}, corresponding to physisorbed N_2 on the OH groups of CZ. The intensity of this band is comparable to that found on CZ (not shown). In addition, a positive contribution is seen at 2110 cm^{-1}. On Rh(1.45)/CZ, however, the negative contribution revealed on CZ at 2139 cm^{-1} is not observed, most likely because of the presence of the broad absorption band (2280–2140 cm^{-1}) peaking at 2192 cm^{-1}. Finally, a very weak absorption band is also present at 2295 cm^{-1} (Fig. 2).

When pulsing O_2, the absorption bands at 2330 and 2295 cm^{-1} remain constant, whereas the contribution at 2110 cm^{-1} decreases drastically, shifts to 2093 cm^{-1}, and becomes negative for a cumulated pulsed quantity of $O_2 > 1.91$ μmol (Fig. 2, spectra c and d). The intensity of the broad band peaking at 2192 cm^{-1} also decreases with the introduction of controlled quantities of O_2. Along with these observations, it is noteworthy that the introduction of small doses of O_2 leads to the appearance of an absorption band of weak intensity at 2244 cm^{-1} for a cumulated pulsed quantity of $O_2 \geqslant 1.91$ μmol (Fig. 2, spectra c and d). Finally, the introduction of O_2 clearly reveals the existence of an isosbestic point located at 2235 cm^{-1} (Fig. 2).

3.2.3. Rh(0.32)/CZ

The adsorption of N_2 at low temperature followed by the introduction of pulsed quantities of O_2 on Rh(0.32)/CZ (Fig. 3) compares qualitatively well with that reported on Rh(1.45)/CZ (Fig. 2). The contributions at 2191 and 2104 cm^{-1} observed for Rh(0.32)/CZ (Fig. 3) are of lower intensities than those found

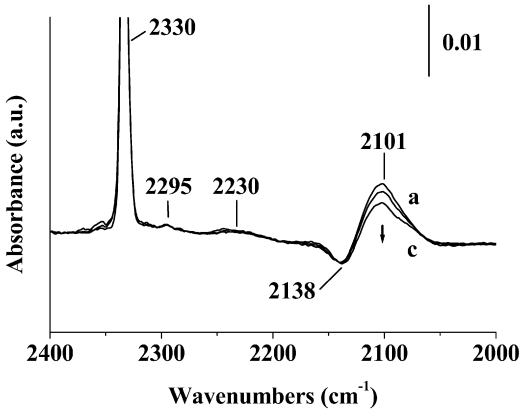

Fig. 4. Low temperature (−173 °C) infrared spectra of the Rh(0.29)/CZ catalyst after adsorption of: (a) N_2 at a pressure of 16.0 Torr and (b, c) subsequent pulses of 1.15 and 0.76 μmol of O_2, respectively.

for Rh(1.45)/CZ (Fig. 2), whereas that at 2295 cm^{-1} seems to be of comparable intensity to that found on Rh(1.45)/CZ. Given the fairly low intensity of this band, this comparison remains challenging, as shown in Fig. 8. As observed on Rh(1.45)/CZ (Fig. 2), the main effect of pulsing O_2 on a N_2-saturated Rh(0.32)/CZ sample is a significant decrease in the intensity of the contributions at 2191 and 2104 cm^{-1}. A negative contribution is also revealed at 2136 cm^{-1} on addition of ⩾3.34 μmol of O_2 (Fig. 3, spectra d–f). It is interesting to note that the intensity of the contribution at 2104 cm^{-1} is similar to that found on CZ and that the appearance of the negative contribution at 2136 cm^{-1} is also in good agreement with that observed on CZ (Fig. 1). Spectrum c (- - -) from Fig. 3 deserves special comment. This spectrum was recorded 40 min after introduction of pulse b. Although additional O_2 was not introduced, the intensity of the contributions at 2191 and 2104 cm^{-1} decreases (Fig. 3). This suggests that the evolution of the N_2 IR features on O_2 adsorption is a relatively slow process under the present experimental conditions. Finally, an absorption band grows at 2244 cm^{-1} with the introduction of O_2, and an isosbestic point is revealed at 2232 cm^{-1} (Fig. 3), as also observed on Rh(1.45)/CZ (Fig. 2).

3.2.4. Rh(0.29)/CZ

Despite the fact that the IR features at 2330, 2295, 2138, and 2101 cm^{-1} observed on Rh(0.29)/CZ (Fig. 4) resemble those already found on CZ, Rh(1.45)/CZ, and Rh(0.32)/CZ (Figs. 1–3), the 2280–2140 cm^{-1} spectral region, within which only a broad absorption band of very weak intensity centered at 2230 cm^{-1} can be distinguished (Fig. 4), differs strikingly from those of Rh(1.45)/CZ and Rh(0.32)/CZ (Figs. 2 and 3). Apart from the contribution at 2101 cm^{-1}, which decreases, the spectra are unaffected when pulsed quantities of O_2 are introduced (Fig. 4).

3.3. CO oxidation

Fig. 5 shows that the temperature-transient CO–O_2 experiment performed on Rh(0.32)/CZ is comparable, within the limits of experimental accuracy, to that reported previously on

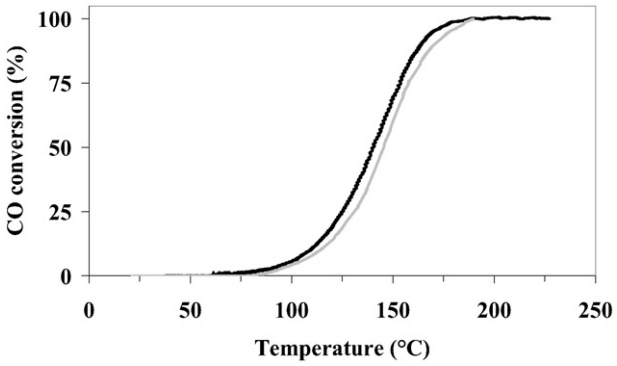

Fig. 5. CO–O_2 temperature-programmed reactions (3 °C min^{-1}, 0.4–0.2% in He, 230 mL_{NTP} min^{-1} total flow rate) on 0.2 g of catalyst sample: (—) Rh(0.32)/CZ or (—) Rh(0.29)/CZ.

Table 2
Comparison of the kinetic parameters associated to the CO–O_2 reaction rate $r = k_0 \exp(-E_a/RT) P_{CO}^{\alpha} P_{O_2}^{\beta}$ estimated on Rh(0.32)/CZ with those reported previously on Rh(0.29)/CZ [17]

Catalysts	α	β	E_a (kJ mol^{-1})	Benzene hydrogenation activity (10^{-6} mol s^{-1} g_{Rh}^{-1})	
				Reduced at 500 °C	Post-catalysis
Rh(0.29)/CZ[a]	0.4	0.1	117	65	48
Rh(0.32)/CZ[b]	0.4	0.0	91	622	384

[a] Synthesized from uncalcined $Ce_{0.68}Zr_{0.32}O_2$.
[b] Synthesized from $Ce_{0.68}Zr_{0.32}O_2$ calcined at 500 °C for 2 h.

Rh(0.29)/CZ [17]. On both catalysts, CO oxidation starts at about 80 °C and is achieved at 190 °C. The temperature of half conversion of CO (T_{50}) is 140 and 145 °C for Rh(0.32)/CZ and Rh(0.29)/CZ, respectively. Under identical experimental conditions, it is noteworthy that CO oxidation starts at much higher temperatures (∼250 °C) on CZ (not shown). This agrees well with previous studies showing that CO oxidation occurs at elevated temperatures on CeO_2 [9,48,49], and confirms that the observed CO oxidation activities of Rh(0.29)/CZ and Rh(0.32)/CZ at low temperatures are not due to CZ alone.

The CO–O_2 kinetic results obtained on Rh(0.32)/CZ are listed in Table 2. As was the case on Rh(0.29)/CZ [17], the reaction orders in CO and O_2 are 0.4 and close to 0, respectively, and the apparent activation energy is close to 100 kJ mol^{-1} for Rh(0.32)/CZ. Table 2 also shows that the benzene hydrogenation activities decrease by about 30–40% after the CO–O_2 reaction. It must be emphasized, however, that the hydrogenation activities estimated on Rh(0.32)/CZ are always one order of magnitude greater than those determined on Rh(0.29)/CZ (Table 2).

4. Discussion

Before discussing the attribution of the IR features observed on the studied samples (Figs. 1–4), we must emphasize that the contribution at about 2100 cm^{-1} corresponds not to N_2 species chemisorbed on Rh, but rather to the forbidden $^2F_{5/2} \rightarrow {}^2F_{7/2}$ electronic transition of Ce^{3+} [50]. After reduction of ceria-related materials, this band is usually observed at 2120 cm^{-1}

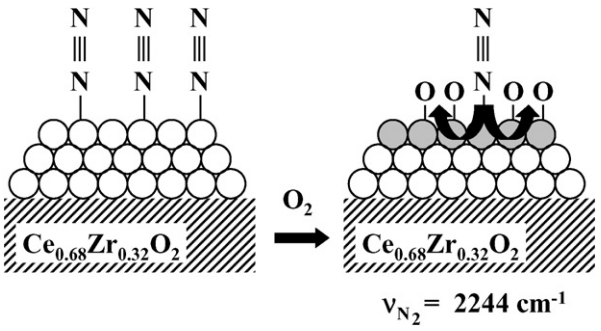

Fig. 6. Schematic representation of the influence of O_2 addition on a Rh crystallite whose exposed surface was contacted with N_2. (○) Rh^0 sites, (◯) $Rh^{\delta+}$ sites. For the sake of simplicity, N_2 chemisorbed species were assumed to adsorb via an end-on configuration and the dissociative adsorption of O_2 was only considered. The arrows represent electron delocalization.

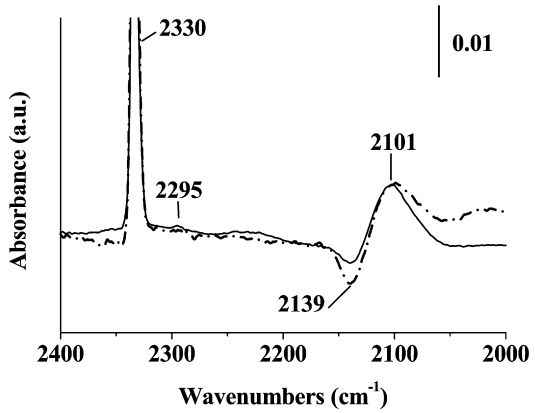

Fig. 7. Comparison of CZ (····) and Rh(0.29)/CZ (—) after exposure to 16.2 and 16.0 Torr of N_2 at –173 °C, respectively.

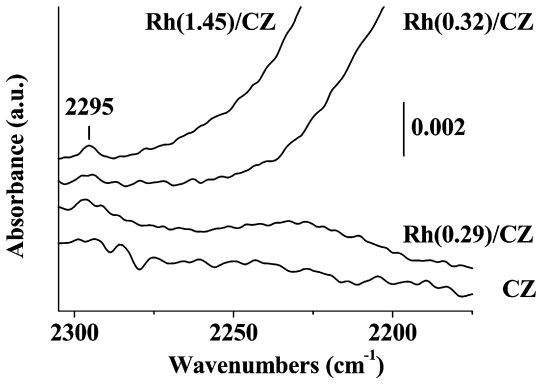

Fig. 8. Low temperature (−173 °C) infrared spectra of CZ, Rh(0.29)/CZ, Rh(0.32)/CZ and Rh(1.45)/CZ after adsorption of 18.2, 16.0, 16.0, and 16.2 Torr of N_2, respectively.

when the spectra are recorded at room temperature [23,50]. The appearance of this band at lower wavenumbers with the introduction of N_2 may be due to extra cooling of the CZ-containing wafers via conduction of the N_2 atmosphere, which could not be fully compensated for by introduction of the He pulse. The decreased wafer temperature results in a slight shift of the band at 2120 cm^{-1} to lower wavenumbers and thus to the appearance of negative and positive contributions at higher and lower wavenumbers, respectively (Fig. 1). This conclusion is supported by the fact that the 2100 cm^{-1} contribution is also observed on the Rh-free sample (Fig. 1) and disappears with the introduction of pulsed quantities of O_2 to become negative (Figs. 2 and 3) with corresponding CZ reoxidation.

The broad absorption band peaking at 2192 cm^{-1} on Rh(1.45)/CZ or Rh(0.32)/CZ (Figs. 2 and 3) can be assigned mainly to N_2 species chemisorbed on Rh^0 sites, the presence of which is corroborated by the benzene hydrogenation activities of these catalysts listed in Table 1. As suggested previously on Rh/SiO_2 samples [41], the large width of the N_2–Rh^0 absorption band (∼100 cm^{-1}) may be attributed to a wide variety of Rh^0 adsorption sites due to the polycrystalline nature of the metallic phase when supported on oxide carriers.

The introduction of pulsed quantities of O_2 on Rh(1.45)/CZ or Rh(0.32)/CZ saturated with N_2 chemisorbed species (Figs. 2 and 3) leads to similar band evolutions as those reported recently on Rh/SiO_2 catalysts [41]. The gradual decrease in intensity of the band peaking at 2192 cm^{-1} and the appearance of an absorption band of weak intensity at 2244 cm^{-1}, along with the existence of an isosbestic point at 2235 cm^{-1} (Figs. 2 and 3), can be attributed to the displacement of N_2-chemisorbed species by O_2 (due to its much greater affinity with Rh) and the evolution of one of these N_2 adsorbed species, respectively. Considering the latter transformation, it is likely that one of the N_2 adsorbed species becomes surrounded by oxygen species adsorbed on neighboring Rh centers (as shown in Fig. 6), resulting in appearance of the band at 2244 cm^{-1}. The shift of this band to higher wavenumbers is inferred to electron withdrawal of the oxygen species chemisorbed on the neighboring Rh surface atoms, resulting in a lower back-donation from Rh to the $2\Pi^*$ antibonding orbitals of N_2 and a positive local deficient charge of these Rh sites ($Rh^{\delta+}$) [41].

On Rh(0.29)/CZ, the presence of Rh^0 centers in very low concentrations cannot be discarded, because the negative contribution at 2139 cm^{-1} is less pronounced than for CZ (Fig. 7), and a broad absorption band of weak intensity is seen at 2230 cm^{-1} (Figs. 4, 7, and 8). The very low concentration of Rh^0 sites is also congruent with the very limited benzene hydrogenation activity of this catalyst (Table 1).

On the Rh/CZ catalysts, an absorption band of very weak intensity is observed at 2295 cm^{-1} (Fig. 8). This band, the intensity of which does not seem to vary to a significant extent on the catalysts studied (Fig. 8), may be attributed to N_2 bonded to electron-deficient Rh centers ($Rh^{\delta+}$), as also suggested on Rh/Al_2O_3 samples in earlier studies for bands reported at about 2300 cm^{-1} [45–47]. It is noteworthy that the intensity of this band is fairly comparable to those reported in these earlier works.

To the best of our knowledge, an absorption band assigned to the stretching vibration of N_2 chemisorbed on Rh^0 sites has not yet been reported at such low wavenumbers (2192 cm^{-1}) for supported Rh catalysts. Stretching vibrations of N_2 species bonded to Rh^0 centers supported on SiO_2 or Al_2O_3 have been observed at 2210–2236 cm^{-1} [41,43,44]. The assignment of absorption bands at about 2260 cm^{-1} to N_2–Rh^0 species on highly dispersed Al_2O_3-supported Rh catalysts has been discussed re-

cently [41] and is likely attributable to the stretching vibration of N_2–$Rh^{\delta+}$ species.

On Rh/CZ catalysts, it must be stressed that not only is the main absorption band at 2192 cm^{-1} shifted to lower wavenumbers compared with Rh/SiO_2 samples studied under identical experimental conditions (2212 cm^{-1} [41]), but also the position of the isosbestic point and the absorption band at 2244 cm^{-1}, related to N_2 species chemisorbed on Rh centers surrounded by oxygen adspecies (Fig. 6), undergo a red shift of about 20 cm^{-1}. This red shift is less pronounced for the N_2–$Rh^{\delta+}$ species supported on CZ (2295 cm^{-1}) compared with the Al_2O_3-supported ones (2301–2303 cm^{-1} [45–47]).

As also discussed in the case of CO adsorption followed by FTIR on PGMs interacting with supports of various basicity [51,52], the observed red shift of the N_2 stretching vibrations may be interpreted in terms of a greater back-donation from the Rh adsorption sites to the antibonding orbitals of N_2 caused by the more basic character of CZ compared with SiO_2 or Al_2O_3.

The existence of electron-deficient Rh centers ($Rh^{\delta+}$), as revealed by the absorption band at 2295 cm^{-1} on the Rh/CZ catalysts (Fig. 8), may appear controversial, given the foregoing conclusions. It must be recalled, however, that the CZ-supported samples contain significant amounts of Cl anions (Table 1), and that oxidized PGMs species may be formed by electron withdrawal from the metal clusters due to the inductive effect of neighboring Cl anions [25–28]. In our opinion, the presence of significant amounts of Cl anions justifies the presence of $Rh^{\delta+}$ sites despite the well-established basic character of the CeO_2-related materials [53–55]. Such a conclusion is corroborated by the red shift of the absorption band attributed to the stretching vibration of N_2 bonded to $Rh^{\delta+}$, which is (because of the combination of these two antagonist phenomena—namely, electron withdrawal from Cl^- and electron donation from the CZ support) less pronounced (7 cm^{-1}) than that found for N_2 species chemisorbed on Rh^0 centers (20 cm^{-1}).

It is noteworthy that there exists a good correlation between the intensity of the band peaking at 2192 cm^{-1} (Figs. 2–4, spectra a) and the benzene hydrogenation activities listed in Table 1 (in mol s^{-1} g_{cat}^{-1}). This shows that both techniques allow reliable characterization of the Rh^0 phase and that Rh(0.32)/CZ exposes much more Rh^0 sites than Rh(0.29)/CZ (Table 1; Figs. 3 and 4). The fact that Rh(0.32)/CZ exposes much more Rh^0 sites than Rh(0.29)/CZ reveals that CZ calcination before Rh deposition drastically modifies the fraction of Rh^0 centers. As benzene hydrogenation is structure-insensitive [20], as long as the electronic density of the targeted centers is identical, it can be concluded that the Rh^0 surface area of Rh(0.32)/CZ is one order of magnitude greater than that of Rh(0.29)/CZ (Table 1, in mol s^{-1} g_{Rh}^{-1}).

In contrast, both CO oxidation activity (Fig. 5) and kinetics (Table 2) are very similar on these catalysts, although Rh(0.32)/CZ exposes much more Rh^0 sites than Rh(0.29)/CZ. This clearly indicates that the Rh^0 sites supported on CZ do not catalyze CO oxidation under the present experimental conditions. As the intensity of the band at 2295 cm^{-1}, attributed to N_2 bonded to $Rh^{\delta+}$ centers, does not vary to any significant extent (Fig. 8), these electron-deficient sites likely are the catalytic centers involved in CO oxidation. These conclusions are further supported by the fact that (i) CO oxidation requires higher temperatures on Rh/SiO_2 (which exhibits only Rh^0 sites) than those on the Rh/CZ samples to achieve identical conversions [15], and (ii) the CO and O_2 reaction orders estimated on the Rh/CZ catalysts are clearly different from those expected for Rh^0 catalytic centers, −1 and +1 with respect to CO and O_2, under experimental conditions for which the Rh^0 surface is covered mainly by CO adspecies [6,15,17,56–59]. Moreover, it is noteworthy that the reaction orders determined in the present study on the Rh/CZ catalysts (Table 2)—+0.4 and ∼0 in CO and O_2, respectively—are in excellent agreement with those found by Yu Yao [6]. This author indeed reported a positive order with respect to CO and a near-0th order with respect to O_2 on oxidized PGMs catalytic sites and claims that the formation of these oxidized centers is promoted by the presence of CeO_2 on the Al_2O_3 support. Even though the kinetic parameters listed in Table 2 are in good agreement with the conclusions drawn by Oh and Eickel or Bunluesin et al. [7,9] on CeO_2-containing catalysts about (i) the suppression of the inhibition effect of CO, (ii) a decreased sensitivity of the reaction rate to gas-phase O_2 concentration, and (iii) a decrease in the apparent activation energy compared with those reported for the Rh^0 sites [6,15,17,56–59], our reaction orders are substantially different from those reported by these authors, 0 and +0.4 with respect to CO and O_2 [7,9]. These differences may be due to the coexistence of $Rh^{\delta+}$ and Rh^0 centers on the catalysts studied by the latter authors, as demonstrated by the presence of an absorption band at 2060 cm^{-1} characteristic of the stretching vibration of CO linearly bonded to Rh^0 sites [7] or changes in the reaction orders at very low CO pressures, leading to values congruent with those expected from Rh^0 centers [9]. In these studies [7,9], the estimated reaction orders thus reflect the contribution of both sites to the reaction rate, which explains that these reaction orders (0/CO and +0.4/O_2) are included between those generally accepted for Rh^0 sites (−1/CO and +1/O_2) [6,15,17,56–59] and those determined for $Rh^{\delta+}$ centers (+0.4/CO and ∼0/O_2) [17].

The fact that the concentration of $Rh^{\delta+}$ sites remains almost constant on the low-loaded Rh/CZ samples, whereas the concentration of Rh^0 sites increases dramatically on Rh(0.32)/CZ (Figs. 3 and 4 and Table 1) remains puzzling, as it seems that this increase in the concentration of Rh^0 sites does not occur at the expense of any other Rh species detectable through benzene hydrogenation or N_2-FTIR. The much lower benzene hydrogenation activity and N_2 chemisorption on Rh(0.29)/CZ cannot be attributed to decoration or alloying effects of the Rh phase with the support, as it has been clearly demonstrated that these phenomena, associated with the so-called SMSI effect, occur only on ceria-related Rh catalysts reduced at temperatures well above 500 °C [60,61]. A more likely explanation for this annoying observation on Rh(0.29)/CZ is the existence of Rh species that neither catalyze benzene hydrogenation nor chemisorb N_2. We emphasize that such species also would not be reactive for CO oxidation, as the CO oxidation kinetics and activity of Rh(0.29)/CZ are comparable to those of Rh(0.32)/CZ (Table 2, Fig. 5).

Two hypotheses may be considered to account for the lack of reactivity of such Rh species of Rh(0.29)/CZ in benzene hydrogenation. First, the formed nanoparticles in a zero-valent state (Rh^0) are too small to catalyze benzene hydrogenation. Puddu and Ponec [62] concluded that the larger Pt ensembles necessary for hydrogenation of benzene were missing on the most dilute Pt–Au alloys, thus explaining the fairly low hydrogenation activity of these alloys. Later, Fuentes and Figueras [63] attributed the decrease in benzene hydrogenation turnover numbers of the most dispersed Rh/Al_2O_3 catalysts to the lower activity of the smallest Rh particles. Such a conclusion also was reached by Pajares et al. [64] about 1-hexene hydrogenation on Rh/SiO_2 catalysts or by Gates and co-workers [65,66] on toluene hydrogenation on supported Ir or Rh/faujasites catalysts. In the latter works, however, the authors could not rule out the possibility of an electronic effect of the support on the PGM nanoparticles.

On the other hand, such a size effect of the CZ-supported Rh clusters does not account for the near-absence of N_2 chemisorption on Rh(0.29)/CZ (Fig. 4), considering that the Rh nanoparticles are in their zero-valent form. In the case of very small clusters, an interaction with the support, with electron transfer from one to another [24,67,68], also may be considered. As mentioned previously, owing to the basic character of CZ, the electron density of these Rh clusters would be increased. To the best of our knowledge, the presence of negatively charged PGMs clusters supported on ceria-related materials has never been considered. Very recently however, Tabakova et al. [69] provided evidence of small negatively charged gold clusters supported on reduced CeO_2. In the case of a series of Pt/faujasite catalysts, for which the electron density of the Pt clusters has been tailored by controlled addition of Na^+ or Cs^+, de Mallmann and Barthomeuf [70] clearly demonstrated that the turnover frequency of benzene hydrogenation decreases as the basicity of the zeolite increases, and hence as the electron density of the Pt clusters increases. Later, Ramaker et al. [71] reported a similar trend for tetralin hydrogenation on Pt/Y samples. Therefore, an increase in the electron density of the studied CZ-supported Rh clusters would account for their much lower benzene hydrogenation reactivity. The decreased hydrogenation reactivity of these electron-enriched Rh clusters may be correlated to (i) the unfavored adsorption of the electron-rich benzene molecule and (ii) the difficulty of H addition to the benzene ring, due to the greater Pt–H bond strength on supports of increased basicity [65,72] and/or the greater hydrogen coverage of the electron-rich nanoparticles [72,73]. It is noteworthy that this increased electron density of the Rh clusters also would account for the unfavored adsorption of weak bases such as N_2 or CO [42], and thus the lack of N_2 adsorption or CO oxidation, respectively, on these electron-enriched clusters on Rh(0.29)/CZ.

The formation of electron-enriched Rh clusters on Rh(0.29)/CZ or of metallic clusters (Rh^0) on Rh(0.32)/CZ obviously lies in the synthesis procedure of the samples and, more particularly, in the significant decrease in the specific surface area of CZ by calcination at 500 °C before Rh deposition for Rh(0.32)/CZ. Because only minor sintering effects are expected for reduction temperatures equal to or lower than 500 °C on CZ-supported materials [4], it is very likely that the more limited specific surface area leads to a decreased dispersion of the Rh phase on Rh(0.32)/CZ, and thus to larger Rh particles than on Rh(0.29)/CZ. This accounts for the lower interaction of these particles with the support and consequently to their more metallic character on Rh(0.32)/CZ, which agrees well with the greater benzene hydrogenation activity found on Rh(0.32)/CZ compared with Rh(0.29)/CZ (Table 1).

5. Conclusion

The characterization of two low-loaded Rh/CZ samples was performed via N_2-FTIR (reported here for the first time, to the best of our knowledge) and benzene hydrogenation before being investigated for CO oxidation activity and kinetics. These samples differ only in the fact that one sample was prepared on CZ in which the specific surface area was decreased before Rh deposition, whereas the second sample was prepared from nonsintered CZ. N_2-FTIR allowed the characterization of both $Rh^{\delta+}$ ($\nu_{N_2} = 2295\ cm^{-1}$) and Rh^0 ($\nu_{N_2} = 2192\ cm^{-1}$) centers. Owing to the basicity of the CZ support, it is noteworthy that the stretching vibrations of the aforementioned N_2 chemisorbed species underwent a red shift compared with those reported previously on SiO_2- or Al_2O_3-supported Rh catalysts. N_2-FTIR revealed that the concentration of $Rh^{\delta+}$ did not vary to a significant extent on both samples, whereas the concentration of Rh^0 sites increased dramatically on Rh(0.32)/CZ, which was prepared from the sintered CZ support. This finding is corroborated by the benzene hydrogenation activity, from which it may be concluded that the Rh^0 surface area of Rh(0.32)/CZ is one order of magnitude greater than that of the sample prepared from the nonsintered CZ (Rh(0.29)/CZ).

In contrast, CO oxidation activity and kinetics are nearly identical on both catalysts. This clearly indicates that under our experimental conditions, CO oxidation is catalyzed not by the Rh^0 centers, but more likely by the $Rh^{\delta+}$ centers. This conclusion is supported by the estimated reaction orders with respect to CO and O_2, which are obviously different from those expected for Rh^0 catalytic sites.

The fact that the concentration of $Rh^{\delta+}$ centers remains apparently constant on both samples and that the dramatic increase in the concentration of the Rh^0 centers on Rh(0.32)/CZ does not seem to occur at the expense of any other Rh species, detectable through benzene hydrogenation or N_2-FTIR, suggests the presence of electron-enriched Rh clusters on Rh(0.29)/CZ, owing to the basicity of CZ. These electron-enriched Rh clusters, which neither catalyze benzene hydrogenation nor chemisorb N_2, do not catalyze CO oxidation either.

Acknowledgments

The Ministère de l'Enseignement Supérieur et de la Recherche supported the work of Dr. C. Fontaine-Gautrelet (grant 8449-2003). The authors thank Professor R. Burch and Dr. F.C.

Meunier for fruitful discussions, and P. Lavaud for technical support.

References

[1] M. Shelef, G.W. Graham, R.W. McCabe, in: A. Trovarelli (Ed.), Catalysis by Ceria and Related Materials, vol. 2, Imperial College Press, London, 2002, chap. 10, p. 343.
[2] D. Duprez, C. Descorme, in: A. Trovarelli (Ed.), Catalysis by Ceria and Related Materials, vol. 2, Imperial College Press, London, 2002, chap. 7, p. 243.
[3] M. Primet, E. Garbowski, in: A. Trovarelli (Ed.), Catalysis by Ceria and Related Materials, vol. 2, Imperial College Press, London, 2002, chap. 13, p. 407.
[4] S. Bernal, J.J. Calvino, J.M. Gatica, C.L. Cartes, J.M. Pintado, in: A. Trovarelli (Ed.), Catalysis by Ceria and Related Materials, vol. 2, Imperial College Press, London, 2002, chap. 4, p. 85.
[5] J.C. Summers, S.A. Ausen, J. Catal. 58 (1979) 131.
[6] Y.F. Yu Yao, J. Catal. 87 (1984) 152.
[7] S.H. Oh, C.C. Eickel, J. Catal. 112 (1988) 543.
[8] C. Serre, F. Garin, G. Belot, G. Maire, J. Catal. 141 (1993) 9.
[9] T. Bunluesin, H. Cortados, R.J. Gorte, J. Catal. 157 (1995) 222.
[10] A. Trovarelli, Catal. Rev. Sci. Eng. 38 (1996) 439.
[11] R.H. Nibbelke, M.A.J. Campman, J.H.B.J. Hoebink, G.B. Marin, J. Catal. 171 (1997) 358.
[12] R.H. Nibbelke, A.J.L. Nievergeld, J.H.B.J. Hoebink, G.B. Marin, Appl. Catal. B Environ. 19 (1998) 245.
[13] J. Kašpar, P. Fornasiero, M. Graziani, Catal. Today 50 (1999) 285.
[14] P. Bera, K.C. Patil, V. Jayaram, G.N. Subbanna, M.S. Hegde, J. Catal. 196 (2000) 293.
[15] I. Manuel, C. Thomas, C. Bourgeois, H. Colas, N. Matthess, G. Djéga-Mariadassou, Catal. Lett. 77 (2001) 193.
[16] K.R. Priolkar, P. Bera, P.R. Sarode, M.S. Hegde, S. Emura, R. Kumashiro, N.P. Lalla, Chem. Mater. 14 (2002) 2120.
[17] I. Manuel, J. Chaubet, C. Thomas, H. Colas, N. Matthess, G. Djéga-Mariadassou, J. Catal. 224 (2004) 269.
[18] F. Fajardie, J.-F. Tempère, J.-M. Manoli, O. Touret, G. Blanchard, G. Djéga-Mariadassou, J. Catal. 179 (1998) 469.
[19] G. Djéga-Mariadassou, F. Fajardie, J.-F. Tempère, J.-M. Manoli, O. Touret, G. Blanchard, J. Mol. Catal. A 161 (2000) 179.
[20] M. Boudart, G. Djéga-Mariadassou, Kinetics of Heterogeneous Catalytic Reactions, Princeton Univ. Press, Princeton, NJ, 1984.
[21] F. Fajardie, J.-F. Tempère, G. Djéga-Mariadassou, G. Blanchard, J. Catal. 163 (1996) 77.
[22] L. Salin, C. Potvin, J.-F. Tempère, M. Boudart, G. Djéga-Mariadassou, J.-M. Bart, Ind. Eng. Chem. Res. 37 (1998) 4531.
[23] C. Fontaine-Gautrelet, J.-M. Krafft, O. Gorce, F. Villain, G. Djéga-Mariadassou, C. Thomas, Phys. Chem. Chem. Phys. 8 (2006) 3732.
[24] S. Bernal, G. Blanco, J.M. Gatica, C. Larese, H. Vidal, J. Catal. 200 (2001) 411.
[25] C. Force, J.P. Belzunegui, J. Sanz, A. Martínez-Arias, J. Soria, J. Catal. 197 (2001) 192.
[26] A. Badri, C. Binet, J.-C. Lavalley, J. Phys. Chem. 100 (1996) 8363.
[27] D.I. Kondarides, X.E. Verykios, J. Catal. 174 (1998) 52.
[28] M.A. Newton, B. Jyoti, A.J. Dent, S.G. Fiddy, J. Evans, Chem. Commun. (2004) 2382.
[29] H.F.J. Van't Blik, J.B.A.D. Van Zon, T. Huizingua, J.C. Vis, D.C. Koningsberger, R. Prins, J. Phys. Chem. 87 (1983) 2264.
[30] F. Solymosi, M. Pástor, J. Phys. Chem. 89 (1985) 4789.
[31] M.I. Zaki, G. Kunzmann, B.C. Gates, H. Knözinger, J. Phys. Chem. 91 (1987) 1486.
[32] G. Bergeret, P. Gallezot, P. Gelin, Y. Ben Taarit, F. Lefebvre, C. Naccache, R.D. Shannon, J. Catal. 104 (1987) 279.
[33] P. Basu, D. Panayotov, J.T. Yates, J. Am. Chem. Soc. 110 (1988) 2074.
[34] T.T.T. Wong, A.Y. Stakheev, W.M.H. Sachtler, J. Phys. Chem. 96 (1992) 7733.
[35] A. Berkó, G. Ménesi, F. Solymosi, J. Phys. Chem. 100 (1996) 17732.
[36] Y.-E. Li, R.D. Gonzalez, J. Phys. Chem. 88 (1984) 898.
[37] J.T. Kiss, R.D. Gonzalez, J. Phys. Chem. 92 (1988) 1589.
[38] D.A. Bulushev, G.F. Froment, J. Mol. Catal. A Chem. 139 (1999) 63.
[39] C. Fontaine-Gautrelet, C. Thomas, J.-M. Krafft, G. Djéga-Mariadassou, Top. Catal., in press.
[40] A. Trovarelli (Ed.), Catalysis by Ceria and Related Materials, vol. 2, Imperial College Press, London, 2002, chap. 2, p. 15.
[41] C. Fontaine-Gautrelet, J.-M. Krafft, G. Djéga-Mariadassou, C. Thomas, J. Phys. Chem. B 110 (2006) 10075.
[42] K. Hadjiivanov, G.N. Vayssilov, Adv. Catal. 47 (2002) 307.
[43] Y.G. Borod'ko, V.S. Lyutov, Kinet. Catal. 12 (1971) 238.
[44] D.J.C. Yates, L.L. Murrell, E.B. Prestridge, J. Catal. 57 (1979) 41.
[45] H.P. Wang, J.T. Yates, J. Phys. Chem. 88 (1984) 852.
[46] J.P. Wey, H.D. Burkett, W.C. Neely, S.D. Worley, J. Am. Chem. Soc. 113 (1991) 2919.
[47] J.P. Wey, W.C. Neely, S.D. Worley, J. Phys. Chem. 95 (1991) 8879.
[48] M. Breysse, M. Guenin, B. Claudel, H. Latreille, J. Véron, J. Catal. 27 (1972) 275.
[49] E. Aneggi, J. Llorca, M. Boaro, A. Trovarelli, J. Catal. 234 (2005) 88.
[50] C. Binet, A. Badri, J.-C. Lavalley, J. Phys. Chem. 98 (1994) 6392.
[51] M.S. Scurrell, J. Mol. Catal. 10 (1981) 57.
[52] D. Barthomeuf, Catal. Rev. Sci. Eng. 38 (1996) 521.
[53] A. Auroux, A. Gervasini, J. Phys. Chem. 94 (1990) 6371.
[54] D. Martin, D. Duprez, J. Mol. Catal. A Chem. 118 (1997) 113.
[55] M.G. Cutrufello, I. Ferino, V. Solinas, A. Primavera, A. Trovarelli, A. Auroux, C. Picciau, Phys. Chem. Chem. Phys. 1 (1999) 3369.
[56] T. Engel, G. Ertl, Adv. Catal. 28 (1979) 1.
[57] N.W. Cant, P.C. Hicks, B.S. Lennon, J. Catal. 54 (1978) 372.
[58] S.H. Oh, G.B. Fisher, J.E. Carpenter, D.W. Goodman, J. Catal. 100 (1986) 360.
[59] S.H. Oh, C.C. Eickel, J. Catal. 128 (1991) 526.
[60] J.M. Gatica, R.T. Baker, P. Fornasiero, S. Bernal, G. Blanco, J. Kašpar, J. Phys. Chem. B 104 (2000) 4667.
[61] S. Bernal, G. Blanco, J.J. Calvino, C. López-Cartes, J.A. Pérez-Omil, J.M. Gatica, O. Stephan, C. Colliex, Catal. Lett. 76 (2001) 131.
[62] S. Puddu, V. Ponec, Rec. Trav. Chim. 95 (1976) 255.
[63] S. Fuentes, F. Figueras, J. Catal. 61 (1980) 443.
[64] J.A. Pajares, P. Reyes, L.A. Oro, R. Sariego, J. Mol. Catal. 11 (1981) 181.
[65] Z. Xu, F.-S. Xiao, S.K. Purnell, O. Alexeev, S. Kawi, S.E. Deutsch, B.C. Gates, Nature 372 (1994) 346.
[66] W.A. Weber, B.C. Gates, J. Catal. 180 (1998) 207.
[67] J.C. Frost, Nature 334 (1988) 577.
[68] C. Hardacre, R. Mark Ormerod, R.M. Lambert, J. Phys. Chem. 98 (1994) 10901.
[69] T. Tabakova, F. Boccuzzi, M. Manzoli, J.W. Sobczak, V. Idakiev, D. Andreeva, Appl. Catal. B Environ. 49 (2004) 73.
[70] A. de Mallmann, D. Barthomeuf, J. Chim. Phys. 87 (1990) 535.
[71] D.E. Ramaker, J. de Graaf, J.A.R. van Veen, D.C. Koningsberger, J. Catal. 203 (2001) 7.
[72] Y. Ji, Ad.M.J. van der Eerden, V. Koot, P.J. Kooyman, J.D. Meeldijk, B.M. Weckhuysen, D.C. Koningsberger, J. Catal. 234 (2005) 376.
[73] M.K. Oudenhuijzen, J.A. van Bokhoven, D.E. Ramaker, D.C. Koningsberger, J. Phys. Chem. B 108 (2004) 20247.